INTERNATIONAL JOURNAL FOR NUMERICAL METHODS IN FLUIDS, VOL. 23, 143–161 (1996)

SINGLE-LAYER FINITE ELEMENT APPROXIMATION OF 3D NAVIER–STOKES EQUATIONS WITH FREE BOUNDARIES FOR SHALLOW WATER FLOWS

GIOVANNI M. CORNETTI

Laboratoire d'Analyse Numérique, Couloir 55–65, 5e Etage, Université Paris 6, 4 Place Jussieu, F-75252 Paris Cedex 05, France

SUMMARY

In order to simulate flows in the shallow water limit, the full incompressible Navier–Stokes equations with free boundaries are solved using a single layer of finite elements. This implies a polynomial approximation of the velocity profile in the vertical direction, which in turn distorts the wave speed. This fact is verified by numerical results: the wave speed depends on the vertical discretization. When at least two layers of finite elements are used, the boundary layer at the bottom can be simulated and the correct solution for the shallow water limit is recovered. Then this algorithm is applied to the prediction of Tsunami event.

KEY WORDS: finite element; incompressible; Navier–Stokes; free surface flows; shallow water

1. INTRODUCTION

Owing to the increasing interest in ecological problems much effort has been devoted in recent years to the mathematical and numerical modelling of the ocean–atmosphere system.[1] The ocean is usually described by means of the 2D shallow water (SW) equations.[2–4] These are derived by the asymptotic expansion in the domain thickness of the Navier–Stokes (NS) equations and are valid in the long-wave limit (see References 5 and 6 for details).

Most of the models assume the hydrostatic pressure approximation to close the system, but, because of this hypothesis, solitary waves are not allowed to be simulated. To describe these phenomena within the SW theory, higher-order terms have to be retained in the 2D asymptotic expansion: a numerical method for solving this problem is discussed in Reference 7.

In this paper the model relies on the finite element discretization of the NS equations via a single layer of elements only in depth. This approach has two main advantages.

1. The approximated solution is obtained by a standard incompressible Navier–Stokes code (e.g. the methods proposed by Hughes *et al.*[8] Pironneau,[9] Patera and coworkers,[10,11] Hansbo,[12] Tezduyar *et al.*[13–15] and Cornetti[16] could be applied).
2. The 3D Navier–Stokes equations with FEM discretization have more mathematical support than the asymptotic analysis, where assumptions on the dependence of the solution on the third co-ordinate may not always be satisfied.

CCC 0271–2091/96/020143–19

Received March 1995
Revised November 1995

The single-layer discretization is equivalent to imposing a linear profile on the velocity in the water depth. For the zero-viscosity case, i.e. for the incompressible Euler equations with free boundary, the related 2D equations are derived from the weak formulation. They do not coincide with the 2D SW system: they lead to similar phenomena such as wave propagation on the free surface, but with different wave speed. However, the phase speed may be corrected by using a non-linear velocity profile. In the limit of constant velocity along the layer the classical value for the long-wave limit is recovered.

The characteristic–Galerkin method to solve the NS with free boundary problem has been discussed in Reference 16 (see also References 17 and 18 for an overview). The domain is decomposed into tetrahedral elements and convection is performed along the trajectories. In Section 3, for the solitary wave test problem, numerical results confirm the dependence of the wave propagation speed on the velocity profile. Moreover, a boundary layer appears at the bottom of the domain if a finer discretization is used.

The correct behaviour, at a reasonable price, is recovered via two layers of finite elements, where the lowest one takes into account the high velocity gradients near the wall. An application of this procedure to propagating fronts generated by earthquakes on the sea bottom, tsunamis, is proposed in Section 4.

Alternatively, as suggested by the derivation of the 2D equations, the discretization by a single layer of brick or pentagonal elements, with a discrete function space using z^a (z is the vertical co-ordinate and a a parameter), could be employed.

2. SINGLE-LAYER FINITE ELEMENT APPROXIMATION OF NAVIER–STOKES EQUATIONS (SLNS)

In order to compare other shallow water models with our approach, we discretize in depth only (i.e. along the vertical direction) the incompressible NS equations with free boundaries. This leads to two-dimensional equations.

From now on we systematically adopt the following rules: italic indices $i, j, \ldots$ take values in the set $\{1, 2, 3\}$; Greek indices $\alpha, \beta, \ldots$ take values in the set $\{1, 2\}$. The repeated index summation convention is used in conjunction with these rules.

2.1. Linear velocity discretization

The velocity profile is assumed to be linear in z (see Figure 1) and the augmented pressure.

$$p' = p + gz$$

constant along the layer

$$\Omega(t) = \{\mathbf{x} = (\mathbf{y}, z): \mathbf{y} \in \omega \subset \mathbb{R}^2, 0 < z < h(\mathbf{y}, t)\}.$$

Therefore the following associated problem may be stated.

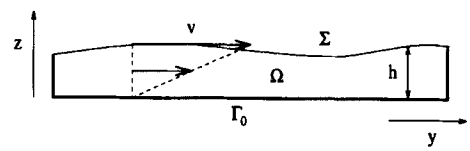

Figure 1. Geometry of fluid layer with imposed linear velocity profile

Find $\mathbf{u} \in V_h$ and $p' \in Q_h$ such that for all $\mathbf{v} \in V_h$ and for all $q \in Q_h$ we have

$$\begin{aligned} &\int_\Omega (\partial_t u_i + u_j \partial_j u_i) v_i - \int_\Omega \partial_i v_i p' + \nu \int_\Omega \partial_j u_i \partial_j v_i = -\int_\Sigma g z v_i n_i + \nu \int_\Sigma \partial_j u_i v_i n_j, \\ &\int_\Omega \partial_j u_j q = 0, \end{aligned} \tag{1}$$

with

$$\begin{aligned} V_h &= \{\mathbf{v} = 2z\bar{\mathbf{v}}/h;\ \bar{\mathbf{v}} \in L^2(0, T; H^1(\omega)^2),\ 0 < z < h(\mathbf{y}, t),\ \mathbf{y} \in \omega;\ \bar{\mathbf{v}}_\alpha(\mathbf{y}, t) = 0,\ \mathbf{y} \in \partial\omega\}, \\ Q_h &= \{q \in L^2(0, T; L^2(\omega))\}. \end{aligned}$$

The bottom is assumed to be flat, while the free surface equation is $z = h(\mathbf{y}, t)$. On the bottom, no-slip conditions are imposed and the horizontal velocity components vanish on $\partial\omega$. The motion of the free boundary Σ is described by

$$\partial_t h + u_\beta \partial_\beta h = u_3 \quad \text{on } \Sigma. \tag{2}$$

Using a linear profile, we have

$$\partial_t h + 2\bar{u}_\beta \partial_\beta h = 2\bar{u}_3, \tag{3}$$

where $\bar{\mathbf{u}}$ is equal to the mean velocity value in each vertical section:

$$\bar{\mathbf{u}}(\mathbf{y}, t) = \frac{1}{h(\mathbf{y}, t)} \int_0^{h(\mathbf{y},t)} \mathbf{u}(\mathbf{y}, z, t) \mathrm{d}z.$$

To simplify the analysis, the case $\nu = 0$ is considered in the following.

Proposition 1

The incompressible Euler equations with free boundaries, approximated by a linear velocity profile and constant pressure in the vertical direction are equivalent to the following set of equations: mass

$$\partial_t h + \partial_\beta (h\bar{u}_\beta) = 0, \tag{4}$$

horizontal momentum

$$h\partial_t \bar{u}_\alpha + \tfrac{3}{2} h\bar{u}_\beta \partial_\beta \bar{u}_\alpha + \tfrac{1}{2} \bar{u}_\alpha \bar{u}_\beta \partial_\beta h + \tfrac{3}{2}(p' - gh)\partial_\alpha h + \tfrac{3}{4} h \partial_\alpha p' = 0, \tag{5}$$

vertical momentum

$$h\partial_t \bar{u}_3 - \bar{u}_3 \partial_t h + \tfrac{3}{2}(\bar{u}_\beta h \partial_\beta \bar{u}_3 - \bar{u}_3 \bar{u}_\beta \partial_\beta h) + 2\bar{u}_3^2 + \tfrac{3}{2}(gh - p') = 0, \tag{6}$$

where $\bar{u}_3 = \frac{1}{2}\partial_t h + \bar{u}_\beta \partial_\beta h$.

Proof. First consider the mass conservation equation in (1). Using the function spaces V_h and Q_h,

$$\begin{aligned} \int_\Omega \partial_j u_j q &= \int_\omega \int_0^h \partial_\beta u_\beta q + \int_\omega \int_0^h \partial_3 u_3 q \\ &= \int_\omega \frac{h\partial_\beta \bar{u}_\beta - \bar{u}_\beta \partial_\beta h}{h^2} q \mathrm{d}y \int_0^h 2z \mathrm{d}z + \int_\omega 2\frac{\bar{u}_3}{h} q \mathrm{d}y \int_0^h \mathrm{d}z \\ &= \int_\omega (h\partial_\beta \bar{u}_\beta - \bar{u}_\beta \partial_\beta h + 2\bar{u}_3) q \mathrm{d}y = 0. \end{aligned}$$

By means of the free surface condition (3) the previous expression is rewritten as

$$\int_\omega (\partial_t h + \partial_\beta h\bar{u}_\beta)q = 0. \tag{7}$$

Now consider the momentum equation

$$\begin{aligned}\int_\Omega (\partial_t u_i + u_j\partial_j u_i)v_i - \int_\Omega \partial_i v_i p' + \int_\Sigma gzn_i v_i \\ = \int_\Omega (\partial_t u_\alpha + u_\beta\partial_\beta u_\alpha + u_3\partial_3 u_\alpha)v_\alpha - \int_\Omega \partial_\alpha v_\alpha p' + \int_\Sigma gzn_\alpha v_\alpha \\ + \int_\Omega (\partial_t u_3 + u_\beta\partial_\beta u_3 + u_3\partial_3 u_3)v_3 - \int_\Omega \partial_3 v_3 p' + \int_\Sigma gzn_3 v_3 = 0.\end{aligned} \tag{8}$$

The first term in the previous expression yields

$$\begin{aligned}&\int_\Omega (\partial_t u_\alpha + u_\beta\partial_\beta u_\alpha + u_3\partial_3 u_\alpha)v_\alpha \\ &= \int_\omega \frac{h\partial_t\bar{u}_\alpha - \bar{u}_\alpha\partial_t h}{h^2}\frac{\bar{v}_\alpha}{h}\,\mathrm{d}y \int_0^h 4z^2\,\mathrm{d}z + \int_\omega \frac{\bar{u}_\beta}{h}\frac{h\partial_\beta\bar{u}_\alpha - \bar{u}_\alpha\partial_\beta h}{h^2}\frac{\bar{v}_\alpha}{h}\,\mathrm{d}y \int_0^h 8z^3\,\mathrm{d}z + \int_\omega \frac{\bar{u}_3}{h}\frac{\bar{u}_\alpha}{h}\frac{\bar{v}_\alpha}{h}\,\mathrm{d}y \int_0^h 8z^2\,\mathrm{d}z \\ &= \int_\omega \left[\tfrac{4}{3}(h\partial_t\bar{u}_\alpha - \bar{u}_\alpha\partial_t h) + 2(h\bar{u}_\beta\partial_\beta\bar{u}_\alpha - \bar{u}_\alpha\bar{u}_\beta\partial_\beta h) + \tfrac{8}{3}\bar{u}_3\bar{u}_\alpha\right]\bar{v}_\alpha,\end{aligned}$$

where the averaged vertical velocity $\bar{u}_3$ is eliminated using (3):

$$\begin{aligned}&\int_\omega \left[\tfrac{4}{3}(h\partial_t\bar{u}_\alpha - \bar{u}_\alpha\partial_t h) + 2(h\bar{u}_\beta\partial_\beta\bar{u}_\alpha - \bar{u}_\alpha\bar{u}_\beta\partial_\beta h) + \tfrac{8}{3}\bar{u}_3\bar{u}_\alpha\right]\bar{v}_\alpha \\ &= \int_\omega \left(\tfrac{4}{3}h\partial_t\bar{u}_\alpha + 2h\bar{u}_\beta\partial_\beta\bar{u}_\alpha + \tfrac{2}{3}\bar{u}_\alpha\bar{u}_\beta\partial_\beta h\right)\bar{v}_\alpha.\end{aligned}$$

From the divergence term,

$$\int_\Omega \partial_\alpha v_\alpha p' = \int_\omega \frac{h\partial_\alpha\bar{v}_\alpha - \bar{v}_\alpha\partial_\alpha h}{h^2}p'\,\mathrm{d}y \int_0^h 2z\,\mathrm{d}z = \int_\omega (h\partial_\alpha\bar{v}_\alpha - \bar{v}_\alpha\partial_\alpha h)p'.$$

Then, using Green's formula and the fact that the horizontal components of the test function $\bar{v}_\alpha$ vanish on the boundary $\partial\omega$, it follows that

$$\int_\omega (h\partial_\alpha\bar{v}_\alpha - \bar{v}_\alpha\partial_\alpha h)p' = \int_\omega (-2p'\partial_\alpha h - h\partial_\alpha p')\bar{v}_\alpha.$$

The unit normal to the free boundary Σ is given by

$$n = (-\partial_1 h, -\partial_2 h, 1)n_3, \qquad n_3 = \frac{1}{\sqrt{(\partial_\alpha h\partial_\alpha h + 1)}},$$

so that the integral on Σ in (8) is replaced by an integral over the 2D domain ω:

$$\int_\Sigma gzv_\alpha n_\alpha = -\int_\omega 2gh\partial_\alpha h\bar{v}_\alpha.$$

Then for $v_3 = 0$ the horizontal momentum equation is derived as

$$\int_\omega \left(\tfrac{4}{3}h\partial_t\bar{u}_\alpha + 2h\bar{u}_\beta\partial_\beta\bar{u}_\alpha + \tfrac{2}{3}\bar{u}_\alpha\bar{u}_\beta\partial_\beta h\right)\bar{v}_\alpha + \int_\omega (2p'\partial_\alpha h + h\partial_\alpha p')\bar{v}_\alpha - \int_\omega 2gh\partial_\alpha h\bar{v}_\alpha = 0. \tag{9}$$

Applying the same procedure using the test function $v=(0, 0, v_3)$ yields the vertical momentum balance

$$\begin{aligned}
&\int_\Omega (\partial_t u_3 + u_\beta \partial_\beta u_3 + u_3 \partial_3 u_3) v_3 - \int_\Omega \partial_3 v_3 p' + \int_\Sigma g z n_3 v_3 \\
&\quad = \int_\omega \frac{h\partial_t \bar{u}_3 - \bar{u}_3 \partial_t h}{h^2} \frac{\bar{v}_3}{h} \mathrm{d}y \int_0^h 4z^2 \mathrm{d}z + \int_\omega \frac{\bar{u}_\beta}{h} \frac{h\partial_\beta \bar{u}_3 - \bar{u}_3 \partial_\beta h}{h^2} \frac{\bar{v}_3}{h} \mathrm{d}y \int_0^h 8z^3 \mathrm{d}z \\
&\qquad + \int_\omega \left(\frac{\bar{u}_3}{h}\right)^2 \frac{\bar{v}_3}{h} \mathrm{d}y \int_0^h 8z^2 \mathrm{d}z - \int_\omega 2\frac{\bar{v}_3}{h} p' \mathrm{d}y \int_0^h \mathrm{d}z + \int_\omega 2gh\bar{v}_3 \\
&\quad = \int_\omega \left[\tfrac{4}{3}(h\partial_t \bar{u}_3 - \bar{u}_3 \partial_t h) + 2(\bar{u}_\beta h \partial_\beta \bar{u}_3 - \bar{u}_3 \bar{u}_\beta \partial_\beta h) + \tfrac{8}{3}\bar{u}_3^2\right] \bar{v}_3 - \int_\omega 2p'\bar{v}_3 + \int_\omega 2gh\bar{v}_3 = 0. \qquad (10)
\end{aligned}$$

Equations (4)–(6) are obtained by writing the previous expressions (7), (9) and (10) in strong form. □

2.2. *Hydrostatic approximation*

If $u_3 \ll 1$, from equation (6) the hydrostatic approximation

$$p' = gh$$

is recovered. Adding the mass conservation equations multiplied by $\bar{u}_\alpha$ to the horizontal motion equations, the following system is obtained in conservative form:

$$\begin{aligned}
&\partial_t(h\bar{u}_\alpha) + \tfrac{3}{2}\partial_\beta(h\bar{u}_\alpha \bar{u}_\beta) - \tfrac{1}{2}h\bar{u}_\alpha \partial_\beta \bar{u}_\beta + \tfrac{3}{4}gh\partial_\alpha h = 0, \\
&\partial_t h + \partial_\beta(h\bar{u}_\beta) = 0.
\end{aligned} \qquad (11)$$

The unknowns are the two averaged horizontal velocity components $\bar{u}_\alpha$ and the water depth h. The structure of the system (11) is quite similar to the standard shallow water equations

$$\begin{aligned}
&\partial_t(h\bar{u}_\alpha) + \partial_\beta(h\bar{u}_\alpha \bar{u}_\beta) + gh\partial_\alpha h = 0, \\
&\partial_t h + \partial_\beta(h\bar{u}_\beta) = 0,
\end{aligned}$$

except for the numerical coefficients and the third term in the momentum equations.

Linearizing the system around $\bar{u}_\alpha = 0$ and $h = H$, the wave equation for a small fluctuation η of h, $h = H + \eta$, is

$$\partial_t^2 \eta - \tfrac{3}{4}gH\partial_\alpha \partial_\alpha \eta = 0,$$

with the associated wave propagation speed

$$c = \sqrt{(\tfrac{3}{4}gH)},$$

which is not the classical value $c = \sqrt{(gH)}$.

This fact is confirmed by numerical computations as discussed in the related Section 3.2. To overcome this physical inconsistency, a different vertical profile should be imposed.

2.3. *Non-linear velocity discretization*

A more general expression for the velocity could be used,

$$\mathbf{u} = (a+1)\left(\frac{z}{h}\right)^a \bar{\mathbf{u}},$$

where a is a parameter with value between 0 and 1, $a \in]0, 1]$. The boundary layer upper limit h_b, since by definition the velocity in the boundary layer satisfies $|\mathbf{u}| < 0{\cdot}95|\mathbf{u}|_{z=h}$, is given by

$$h_b = 0{\cdot}95^{1/a}h.$$

For $a = 1$ the linear case considered in the previous subsection is recovered. The discrete function spaces for velocity and pressure respectively are

$$V_h = \{\mathbf{v} = (a+1)(z/h)^a\bar{\mathbf{v}};\ \bar{\mathbf{v}} \in L^2(0, T; H^1(\omega)^3),\ 0 < z < h(\mathbf{y}, t),\ \mathbf{y} \in \omega;\ \bar{v}_\alpha(\mathbf{y}, t) = 0,\ \mathbf{y} \in \partial\omega\},$$
$$Q_h = \{q \in L^2(0, T; L^2(\omega))\}.$$

Using the function space V_h, the motion of the free boundary Σ is described by

$$\partial_t h + (a+1)\bar{u}_\beta\partial_\beta h = (a+1)\bar{u}_3.$$

Proposition 2

The incompressible Euler equations with free boundaries, approximated by the function spaces V_h and Q_h, are equivalent to the following system of equations: mass

$$\partial_t h + \partial_\beta(h\bar{u}_\beta) = 0, \tag{12}$$

horizontal momentum

$$\partial_t(h\bar{u}_\alpha) + \frac{(a+1)(2a+1)}{3a+1}\partial\bar{u}_\beta(h\bar{u}_\alpha) - \frac{a(a-1)}{3(3a+1)}\bar{u}_\beta\bar{u}_\alpha\partial_\beta\bar{u}_\alpha - \frac{3a^2+2a+1}{3(3a+1)}\bar{u}_\alpha h\partial_\beta\bar{u}_\alpha$$
$$+ \frac{2a+1}{a+1}(p'\partial_\alpha h - gh\partial_\alpha h) + \frac{2a+1}{(a+1)^2}h\partial_\alpha p' = 0, \tag{13}$$

vertical momentum

$$h\partial_t\bar{u}_3 - a\bar{u}_3\partial_t h + \frac{(a+1)(2a+1)}{3a+1}(h\bar{u}_\beta\partial_\beta\bar{u}_3 - a\bar{u}_3\bar{u}_\beta\partial_\beta h) + \frac{(a+1)(2a+1)}{3}\bar{u}_3^2 + \frac{2a+1}{a+1}(gh - p') = 0, \tag{14}$$

where

$$\bar{u}_3 = \frac{1}{a+1}\partial_t h + \bar{u}_\beta\partial_\beta h.$$

The proof holds in the same way as for Proposition 1.

2.4. Linearized dynamics

In the next proposition the dispersion relation, i.e. the formula that gives the frequency ω as a function of the wave number $|\mathbf{k}| = \sqrt{(k_\alpha k_\alpha)}$, $\omega = \omega(|\mathbf{k}|)$, is written for the linearized equations. They are derived from (12)–(14) without any major hypothesis and incorporate the effect of deviation from hydrostatic balance.

Proposition 3

The dispersion relation associated with the linearized equations of (12)–(14) is

$$\omega^2 = \frac{(2a+1)gH|\mathbf{k}|^2}{(a+1)^2 + H^2|\mathbf{k}|^2}. \tag{15}$$

Proof. The system (12)–(14) is expanded around $\bar{\mathbf{u}} = 0$, $h = H$ and η and $\mathbf{w}$ are the depth and velocity fluctuation respectively:

$$h = H + \eta, \qquad \bar{u}_i = 0 + w_i.$$

The vertical momentum balance (14) gives

$$p' = \frac{1}{2a+1} H \partial_t^2 \eta + gH + g\eta$$

and, replacing the previous expression in the horizontal equations of motion (13),

$$\begin{aligned} &H\partial_t w_\alpha + \frac{2a+1}{(a+1)^2} gH\partial_\alpha \eta + \frac{1}{(a+1)^2} H^2 \partial_\alpha \partial_t^2 \eta = 0, \\ &\partial_t \eta + H\partial_\beta w_\beta = 0, \end{aligned} \tag{16}$$

where also the mass conservation equation is considered. The variable w_α is eliminated from (15) and the system is reduced to

$$\partial_t^2 \eta - \frac{2a+1}{(a+1)^2} gH\partial_\alpha \partial_\alpha \eta - \frac{1}{(a+1)^2} H^2 \partial_\alpha \partial_\alpha \partial_t^2 \eta = 0. \tag{17}$$

Substituting the periodic travelling wave form of the solution

$$\eta = \eta_0 \exp[\mathrm{i}(k_\alpha x_\alpha - \omega t)]$$

yields the dispersion relation (15). □

Remark 1

The wave equation (17) looks similar to the one described by Camassa and Holm[6] in the absence of stratification, for instance due to a salinity gradient, where the term

$$H^2 \partial_\alpha \partial_t^2 \eta = H^2 \partial_t \partial_\alpha (\partial_\beta w_\beta)$$

in (16) represents the non-hydrostatic dispersion effect.

Figure 2 shows a comparison between the adimensionalized phase speed

$$c' = \frac{c}{\sqrt{(gH)}}, \qquad c = \frac{\omega}{|\mathbf{k}|},$$

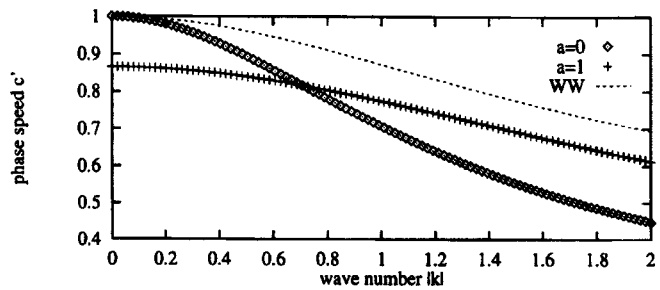

Figure 2. Adimensionalized phase speed c' for SLNS and WW equations as a function of wave number $|\mathbf{k}|$. The depth is set to $H = 1$

as a function of the wave number $H|\mathbf{k}|$, for equation (13) and for the relation

$$\omega^2 = g|\mathbf{k}| \tanh(H|\mathbf{k}|)$$

associated with the linearized water wave (WW) equations (see Reference 5 for the derivation). In the long-wave limit $H|\mathbf{k}| \to 0$ the SLNS equation for $a = 0$ is now, with a constant horizontal velocity profile, physically correct. The global behaviour could be recovered by tuning the parameter a. For instance, for $a = 1$ the dispersion relation related to the WW equations is well approximated in the medium-wave range.

3. NUMERICAL SIMULATION

The numerical scheme to solve the incompressible Navier–Stokes equation with free boundary in the single-layer case has been discussed in Reference 16. Briefly, a splitting technique is used: first by the method of characteristics the total derivative and the free surface position are computed, then an implicit Stokes problem is solved on the new domain. Mesh points on the surface are moved in the vertical direction only and tetrahedral elements with function spaces $P1 + bubble$ for velocity and $P1$ for pressure discretization are used in order to satisfy the Babuska–Brezzi condition for the Stokes problem. The method is employed to simulate the dynamics of a solitary wave as a test problem. For comparison the solutions using several layers of finite elements are given also.

3.1. Solitary wave test problem

For inviscid flows the free surface dynamics may be described by the Korteg de Vries (KdV) equation in the limit of a long-wave and small-amplitude perturbation:

$$\mu = |\mathbf{k}|H \ll 1, \qquad \epsilon = \frac{\eta}{H} \ll 1,$$

where $|\mathbf{k}| = 2\pi/\lambda$ is the wave number and λ is the wavelength. The mean surface elevation H is displayed in Figure 3. The KdV equation has an analytical solution, called a soliton, represented by a single peak propagating in time (for an overview of the KdV and other SW equations see Reference 5). The surface displacement is given by

$$\eta = A \operatorname{sech}\left(\frac{x - ct}{\lambda}\right), \tag{18}$$

with

$$c = \sqrt{[gH(1 + \epsilon)]}$$

the wave propagation velocity, A a constant and sech the hyperbolic secant function.

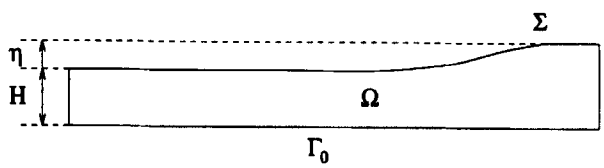

Figure 3. Geometry of fluid layer in initial configuration for solitary wave test problem. The free boundary Σ and the boundary part with no-slip condition, Γ_0 are shown

Using the previous algorithm, the propagation of a solitary wave in a constant depth channel is computed. As initial condition the velocity is set to zero and the free boundary profile is given. On the side wall a slip condition is imposed in the vertical direction, while a no-slip condition is assumed for the bottom. Figure 4 displays the mesh used for the single-layer case.

Numerical data are listed below:

horizontal domain	$\omega =]0,\ 100[\times]-5,\ 5[$
initial velocity	$\mathbf{u} = 0$
acceleration due to gravity	$\mathbf{g} = 1$
initial free boundary profile	$\eta(y_1, y_2) = 0{\cdot}01\ \mathrm{sech}(y_1/8)$
water depth	$H = 1$
time step	$k = 2$

The expected wave propagation speed is

$$c = \sqrt{[gH(1+\epsilon)]} \approx 1.$$

3.2. *Computed results*

Figure 5 shows the behaviour of the solitary wave in time. Only a single layer of finite elements is used and a linear velocity profile is recovered in the vertical direction. The wave top conserves one half of the initial elevation, so that part of the potential energy is transformed into kinetic energy. Owing to the high Reynolds number, $Re = 1000$, the wave is moving without being flattened by viscosity.

A finer discretization, using more layers of finite elements in the vertical direction (see Figure 6), displays a rapid growth of the horizontal velocity near the bottom, while the profile remains constant in the rest of the domain: a boundary layer appears. In Figure 7, to get a better result, the mesh is refined in the high-gradient region. Applying the same number of layers as in the previous case, the horizontal velocity variation is now confined to a narrower part which depends on the size of the lower layer.

For practical application a two-layer discretization would be sufficient. In particular, a thin layer is employed in the strong-gradient region. Figures 7 and 8 show almost the same vertical velocity profile, despite only two layers being used in the latter.

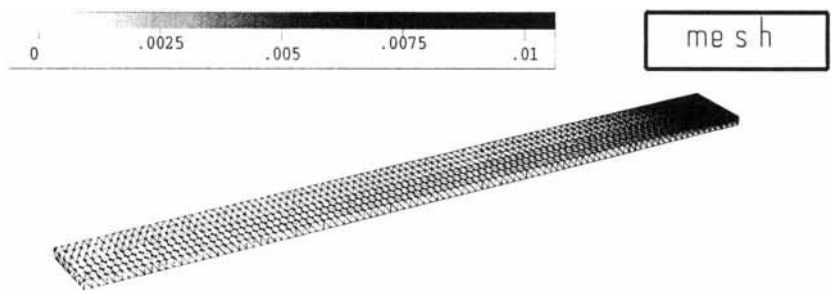

Figure 4. Perspective view of initial mesh. Tetrahedral elements are placed in a single layer. Grey tones on the top surface indicate the displacement η

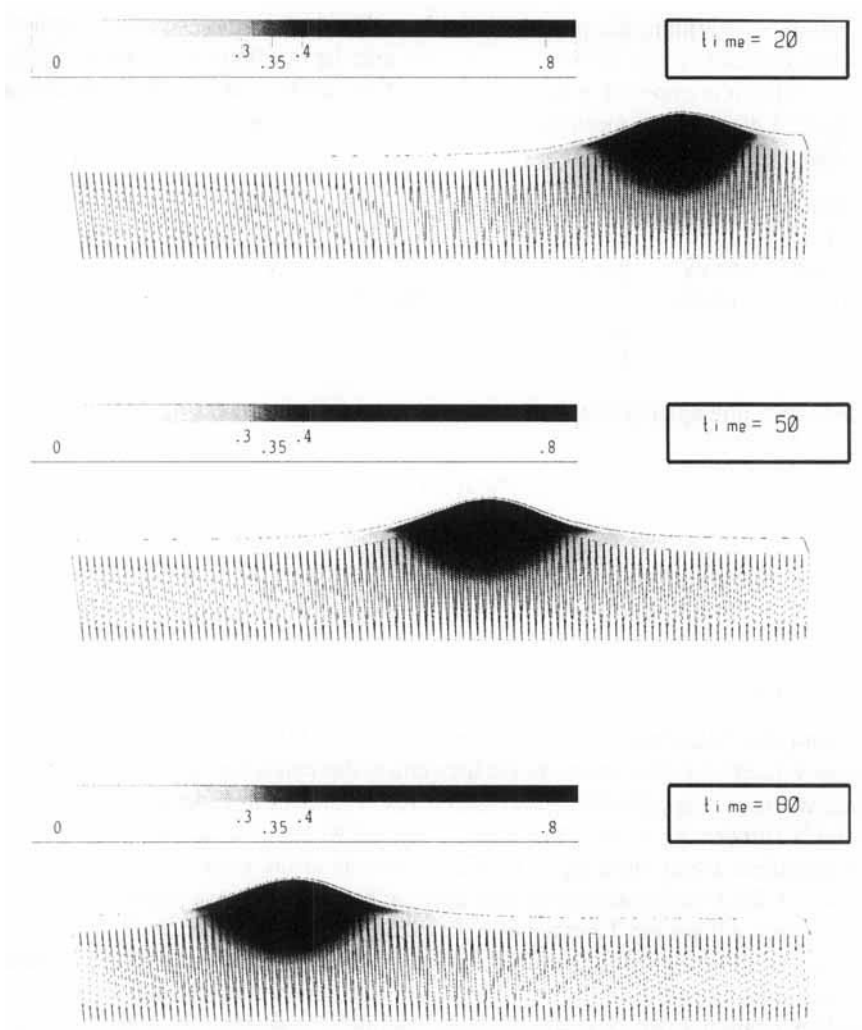

Figure 5. Cut view of test problem solution with single layer of tetrahedral elements at three different times. The surface displacement η is magnified by a factor of 1000 and the layer thickness H by a factor of 10. The horizontal velocity scale is shown (top left)

The distance of the computed water level from the analytical one (see equation (18)) is divided by the amplitude of the solitary wave, $A = 0{\cdot}005$, to obtain the relative L^1 error. This error, represented by Figure 9, decreases with the size of the lower layer of finite elements. Also, the wave speed is measured. The adimensional value $c' = c/\sqrt{(gH)}$ is given below for all four discretization cases:

single layer	0·89
four layers	0·95
four layers + refinement	0·97
two layers + refinement	0·96

The numerical results confirm the dependence of the phase speed on the vertical discretization shown in Section 2. Whenever the mesh grid is refined and well adapted to the solution, the correct phase speed value is achieved in the limit.

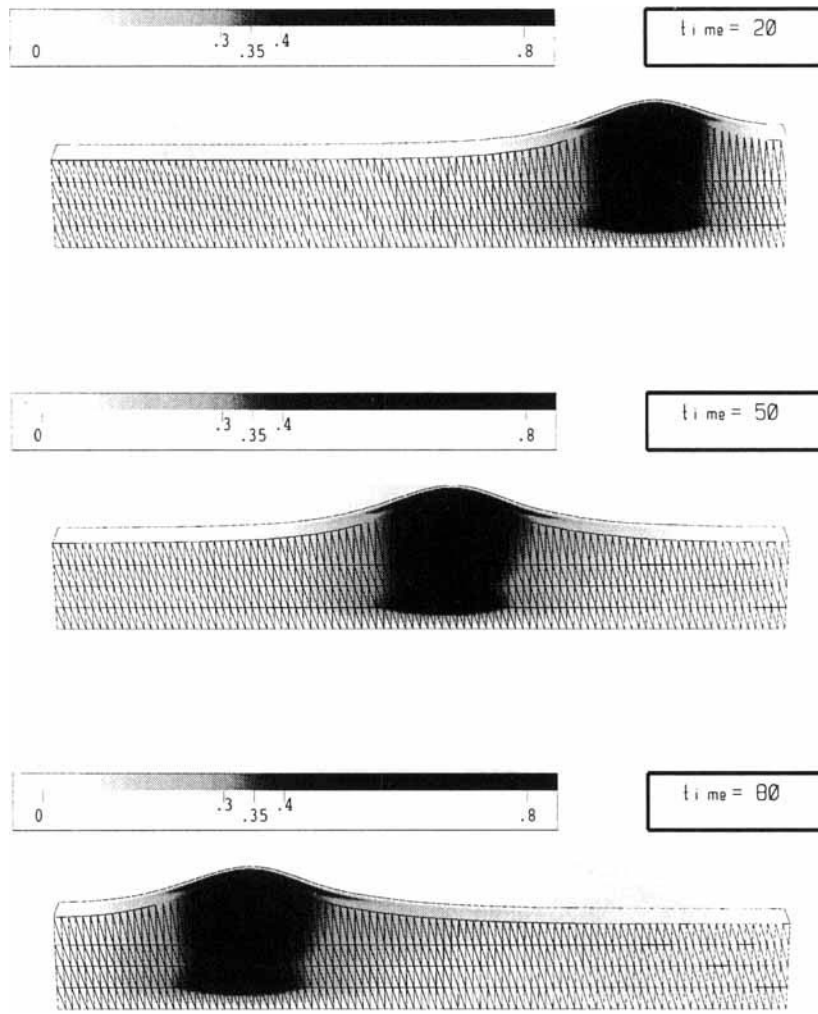

Figure 6. Cut view of solution. The finite elements are placed in four layers of equal size. A boundary layer appears near the bottom wall

The numerical value for the single-layer case is in good agreement with the one obtained for a linear profile under the hypothesis of the validity of the hydrostatic approximation (see Section 2.2):

$$c' = \sqrt{\tfrac{3}{4}} \approx 0{\cdot}87.$$

All tests were performed on an hp9000-735/90 workstation. The corresponding computer times and storage costs are given below:

	memory (kbyte)	computer time (s)
single layer	217	3019
four layers	683	21192
four layers + refinement	683	19298
two layers + refinement	374	11453

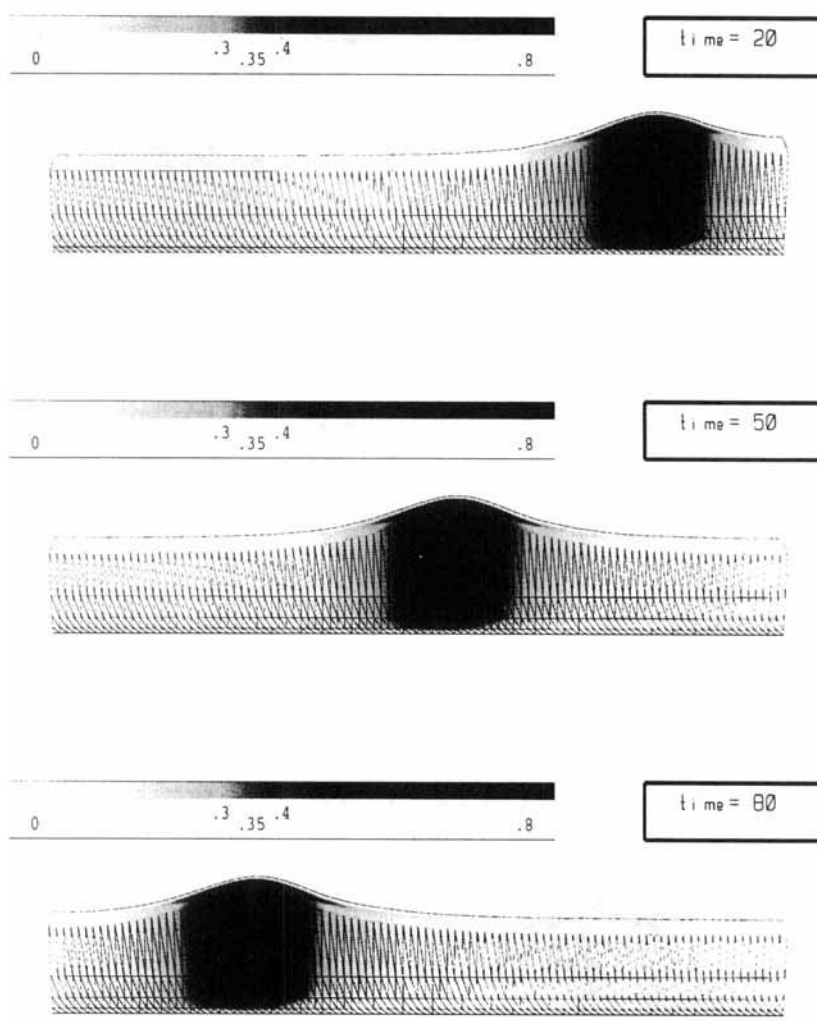

Figure 7. Cut view of solution with four layers of finite elements refined near bottom. The velocity profile is almost constant and the boundary layer is confined to a thin region. $Re = 1000$

4. A PREDICTION OF A TSUNAMI

An earthquake on the sea floor induces an instantaneous motion of the water surface. Despite its usually low amplitude (1 m) in the deep sea, the propagating front can reach a large amplitude near the coast as a consequence of refraction and local topography.

Algeciras Bay in the Mediterranean Sea is used for the simulation of one of these events. The computational domain includes both the bay and the epicentre. It has a characteristic length of about 30 km and the height of the water surface is increased by about 2 m as initial condition at the epicentre.

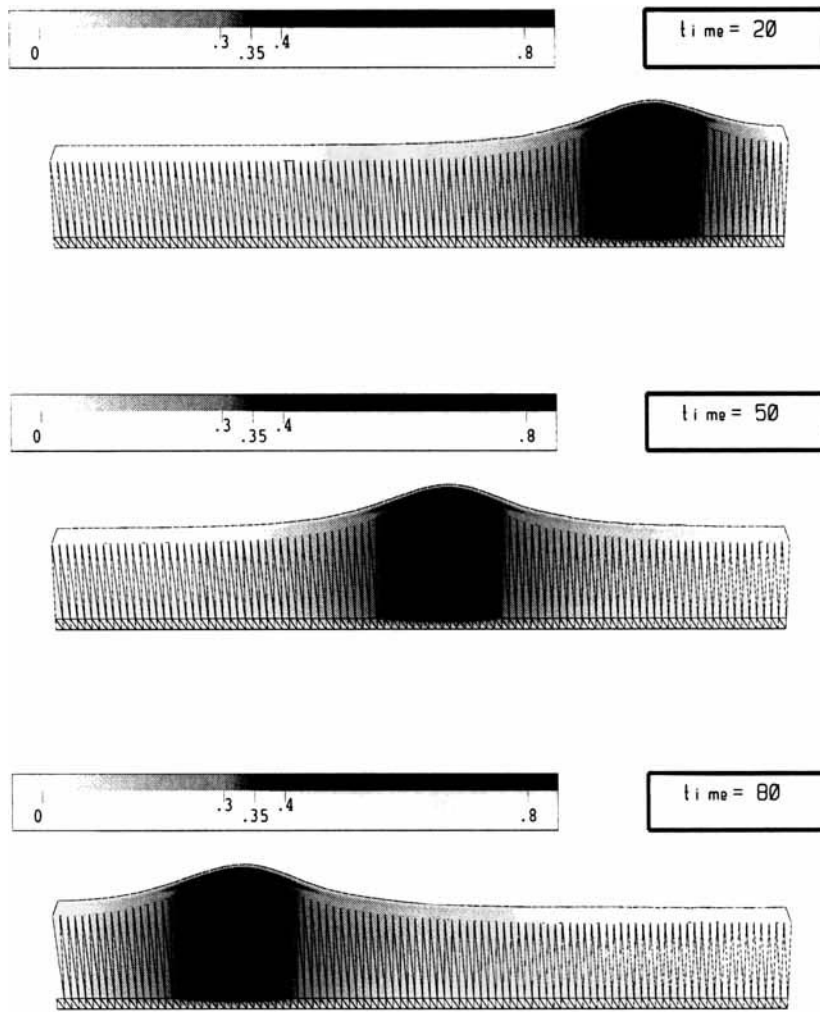

Figure 8. Cut view of solution with two-layer discretization only. The vertical size of the lower layer is 0·125 and the total depth $H=1$. The velocity profile and surface phase speed look almost the same even though a smaller number of elements have been used as in Figure 7

4.1. Boundary conditions

The computational 3D domain is redefined to allow variations in the bottom profile $z=-H(\mathbf{y})$:

$$\Omega(t) = \{\mathbf{x} = (\mathbf{y}, z): \mathbf{y} \in \omega \subset \mathbb{R}^2, \eta(\mathbf{y}, t) > z > -H(\mathbf{y})\},$$

where $z=\eta(\mathbf{y}, t)$ is the equation of the free surface, so that $h=\eta+H$ is the total depth.

As shown in Figure 10, the boundary is decomposed as follows:

$$\partial\Omega(t) = \Gamma_w(t) \cup \Gamma_0 \cup \Sigma(t),$$

side wall $\quad \Gamma_w(t) = \{\mathbf{x} = (\mathbf{y}, z): \mathbf{y} \in \partial\omega, \eta(\mathbf{y}, t) > z > -H(\mathbf{y})\},$

bottom $\quad \Gamma_0 = \{\mathbf{x} = (\mathbf{y}, z): \mathbf{y} \in \omega, z = -H(\mathbf{y})\},$

free surface $\quad \Sigma(t) = \{\mathbf{x} = (\mathbf{y}, z): \mathbf{y} \in \omega, z = \eta(\mathbf{y}, t)\}.$

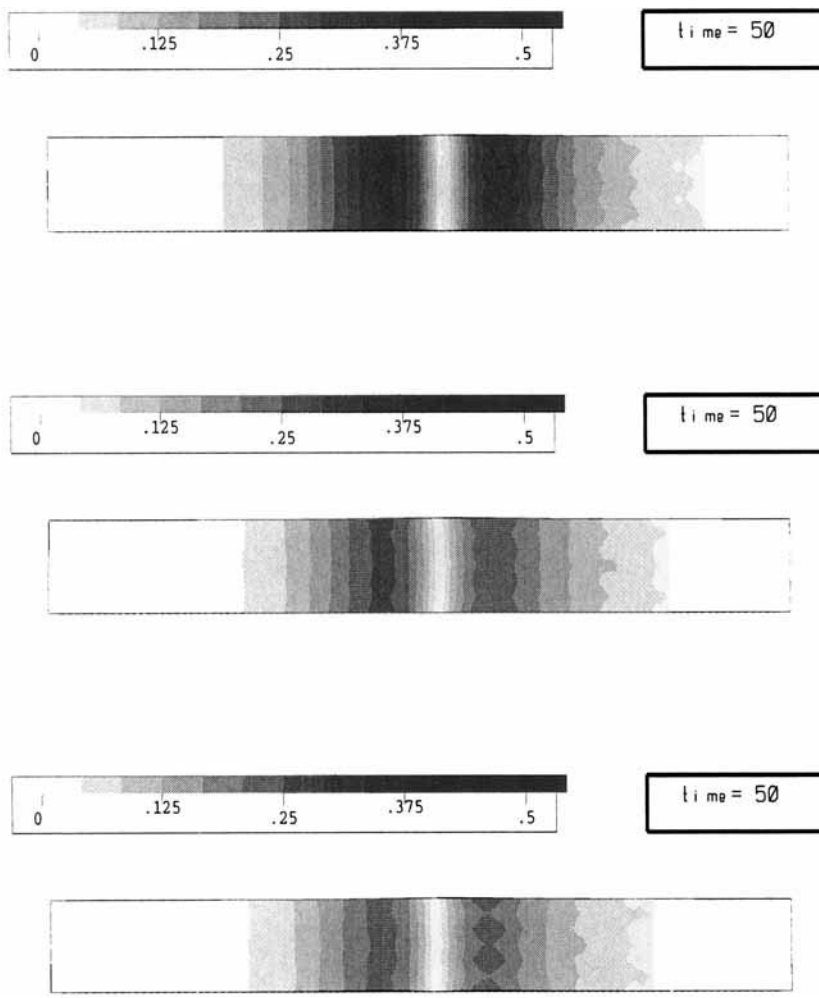

Figure 9. Relative L^1 error of water level with three different meshes at time $t = 50$. From top to bottom: single layer, four layers and two layers with refinement. The results are consistent with the wave speed data. The error decreases when the size of the lower layer of finite elements is reduced

Then the boundary conditions for the 3D incompressible NS equations are applied:

$$\begin{array}{lrll} \text{coast} & (u_1, u_2) = (0, 0),\ \partial_j u_3 n_j = 0 & \text{on} & \Gamma_u(t), \\ \text{open sea} & -\nu \partial_j u_i n_j + (p + gz) n_i = g\eta n_i & \text{on} & \Gamma_p(t), \\ \text{bottom} & \mathbf{u} = 0 & \text{on} & \Gamma_0, \\ \text{free surface} & -\nu \partial_j u_i n_j + (p + gz) n_i = g\eta n_i & \text{on} & \Sigma(t), \end{array}$$

with $\Gamma_w(t) = \Gamma_u(t)\Gamma_p(t)$. Here g is the acceleration due to gravity, ν is the kinematic viscosity and $\mathbf{n}$ is the outward-pointing normal to $\partial\Omega(t)$. At time $t = 0$ the velocity over all the domain is set to zero.

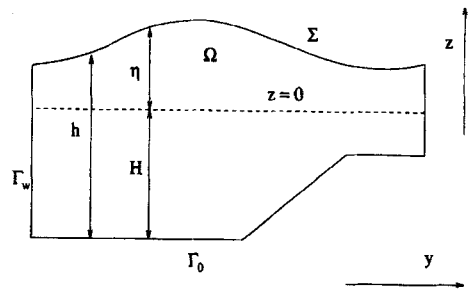

Figure 10. Geometry of fluid layer for tsunami problem

The flow is able to slip along the side wall in the vertical direction. On $\Sigma \cup \Gamma_p$ the surface tension and tangential stresses are neglected and the hydrostatic pressure $p = g\eta$ is imposed. In environmental flows Γ_u represents the shoreline with zero horizontal velocity and Γ_p the open sea. The last condition allows surface waves to radiate out of the domain without being reflected.

4.2. Computed results

The two-layer mesh used for the finite element discretization is shown in Figure 11. The lower layer is only 10 m heigh and therefore is not visible in the figure.

The magnitude of the time step is limited by a CFL condition associated with the wave propagation speed. The minimum horizontal element size $h_T = 500$ m and maximum depth $H_{max} = 500$ m give a bound on the time step:

$$k < \frac{h_T}{\sqrt{(gH_{max})}} \approx 7 \text{ s}.$$

General data for the numerical simulation are listed below:

number of mesh points	2822 × 3
initial velocity	$\mathbf{u} = 0$
acceleration due to gravity	$g = 9{\cdot}8$ m s^{-1}
initial water surface elevation	$\eta_0 = 2$ m
radius of initial water surface perturbation	$r_0 = 3$ km
maximum water depth	$H_{max} = 500$ m
time step	$k = 6$ s

Figures 12–14 display the computed results. Grey tones illustrate surface elevation. The epicentre is located at about 12 km from the coast in a region of 500 m deep water.

The propagating front is reflected by a sudden change in the bottom profile near the coast (compare Figure 13 with the sea bottom topography in Figure 11). Then the maximum surface elevation on the shore is detected close to the two sides of the bay entrance, as shown in Figure 14.

5. CONCLUSIONS

The long-wave shallow water model differs from the single-layer FEM discretization of the NS equations. In the single-layer NS approach the phase speed depends on the velocity profile in the layer depth. To obtain the physically correct phase speed in the long-wave regime, high-order polynomials in the vertical direction have to be used or, alternatively, a two-layer discretization. In these cases the

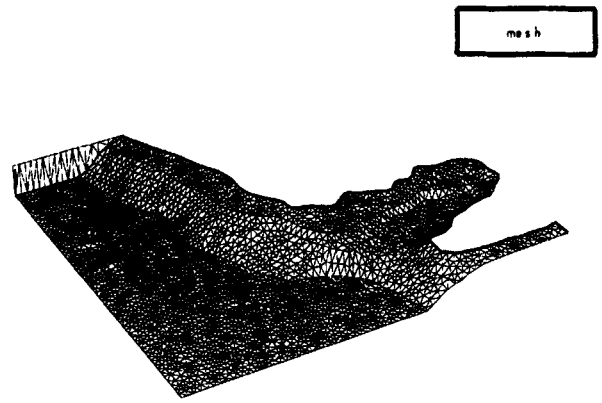

Figure 11. Mesh of sea bottom. The depth is magnified by a factor of five. Tetrahedral elements are placed in two layers; the lower layer is only 10 m high, which is small, since the maximum total depth of the domain is 500 m

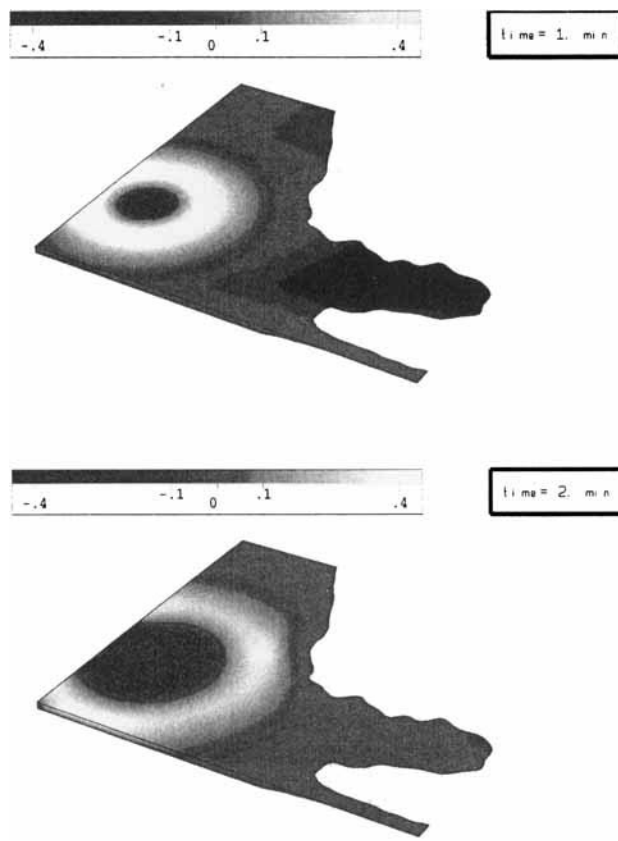

Figure 12. Perspective view of solution for tsunami problem. As initial condition the water level is increased by 2 m at the epicentre, located 10 km off the coast. The surface elevation scale in metres (top left) and the time (top right) are shown

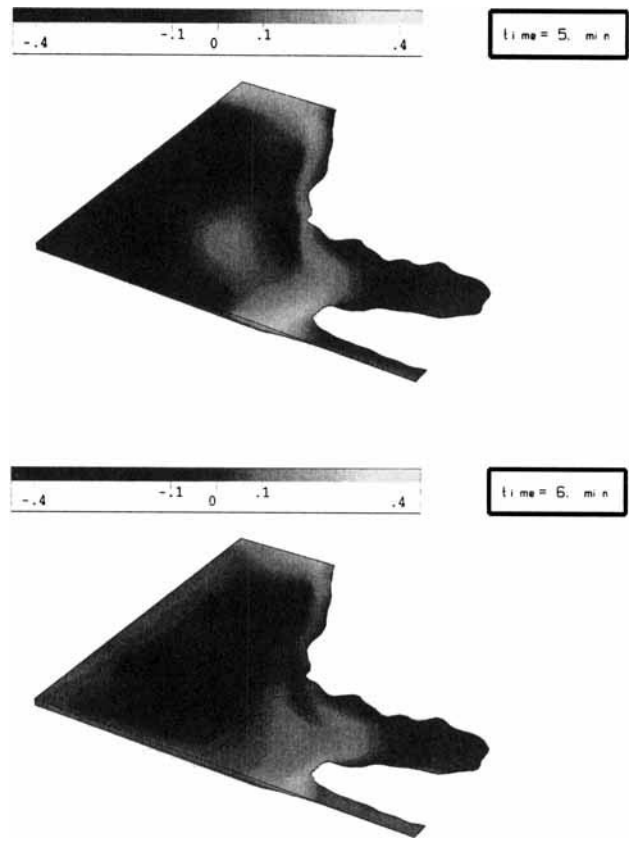

Figure 13. Perspective view of solution for tsunami problem. Before reaching the coast, the wave front is partially reflected by the sudden change in the bottom topography

equivalent of the two-dimensional limit model has the same behaviour as the NS approach, i.e. they display the same phase speed, but at the same time is more general than the shallow water equations, because the hydrostatic approximtaion is not necessary.

ACKNOWLEDGEMENTS

The author is very grateful to Professor Pironneau for his supervision of the entire work. The author also wishes to thank Instituto Español de Oceanografía (Centro Fuengirola) for providing him with general data on the sea bottom topography near Algeciras.

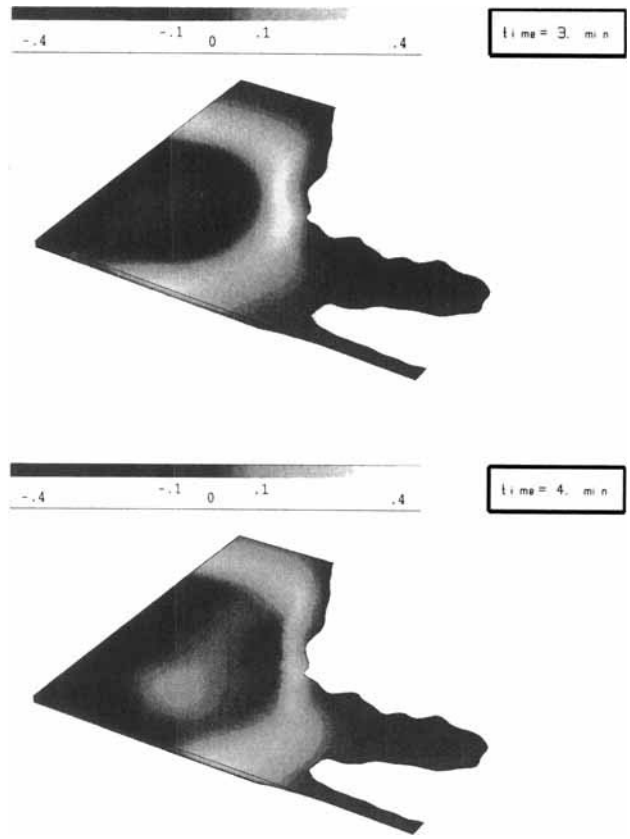

Figure 14. Perspective view of solution for tsunami problem. The maximum surface elevation on the shore is found on each side of the bay entrance

REFERENCES

1. I. Rasol, 'Global change and eco-systems', *Proc. ERCOFTAC Meet.*, Varese, April 1991.
2. V. Agoshkov, E. Ovtchinnikov, V. Pennati, D. Ambrosi and F. Saleri, 'Finite element, finite volume and finite differences approximation to shallow water equations', in *Finite Elements in Fluids CIMNE Barcelona*, Pineridge, Swansea, 1993, pp. 1001–1009.
3. M. J. Castro, C. Pares and J. Macias, 'Numerical modelling of the Alboran sea', in *Finite Elements in Fluids CIMNE Barcelona*, Pineridge, Swansea, 1993, pp. 1081–1092.
4. M. Iskandarini, D. B. Haidvogel and J. P. Boyd, 'A staggered spectral element model with application to the oceanic shallow water equations', *Int. j. numer. methods fluids*, **20**, 393–414 (1995).
5. C. C. Mei, *The Applied Dynamics of Ocean Surface Waves*, World Scientific, Singapore, 1989.
6. R. Camassa and D. Holm, 'Dispersive barotropic equations for stratified mesoscale ocean dynamics', *Physica D*, **60**, 1–15 (1992).
7. J. S. Antunes do Carmo, J. Seabra Santos and E. Barthelemy, 'Surface wave propagation in shallow water: a finite element model', *Int. j. numer. methods fluids*, **16**, 447–459 (1993).
8. T. J. R. Hughes, W. K. Liu and T. K. Zimmermann, 'Lagrangian Eulerian finite element formulation for incompressible flow', *Comput. Methods Appl. Mech. Eng.*, **29**, 329–349 (1981).
9. O. Pironneau, *The Finite Element Method in Fluids*, Masson, Paris, 1989.
10. L. Ho and A. Patera, 'A Legendre spectral element method for the simulation of unsteady incompressible viscous free-surface flows', *Comput. Methods Appl. Mech. Eng.*, **80**, 171–186 (1990).
11. L. Ho, Y. Maday, A. Patera and E. Ronquist, 'An operator integration splitting method for time dependent problems. Application to incompressible fluid flows', *J. Sci. Comput.*, **5**, 263–294 (1990).
12. P. Hansbo, 'The characteristic streamline diffusion method for the time dependent incompressible Navier–Stokes equations', *Comput. Methods Appl. Mech. Eng.*, **99**, 355–366 (1992).

13. T. E. Tezduyar, M. Behr and J. Liou, 'A new strategy for finite element computations involving moving boundaries and interfaces—the DSD/ST procedure: I. The concept and the preliminary numerical tests', *Comput. Methods Appl. Mech. Eng.*, **94**, 339–351 (1992).
14. T. E. Tezduyar, M. Behr, S. Mittal and J. Liou, 'A new strategy for finite element computations involving moving boundaries and interfaces—the DSD/ST procedure: II. Computations of free-surface flows, two liquid flows, and flows with drifting cylinders', *Comput. Methods Appl. Mech. Eng.*, **94**, 353–371 (1992).
15. T. E. Tezduyar, 'Stabilized finite element formulations for incompressible flow computation', *Adv. Appl. Mech.*, **28**, 1–44 (1992).
16. G. M. Cornetti, 'A characteristic–Galerkin method for the Navier– Stokes equations in thin domains with free boundaries', in *Modelling, Mesh Generation and Adaptive Numerical Methods for Partial Differential Equations*, vol. 75, 201–213, Springer, New York, 1995.
17. O. Pironneau, J. Liou and T. Tezduyar, 'Characteristic Galerkin and Galerkin least squares space time formulations for the advection diffusion equation with time dependent domains', *Comput. Methods Appl. Mech. Eng.*, **100**, 117–141 (1992).
18. K. Boukir, Y. Maday and B. Metivet, 'A high order characteristic finite element method for the incompressible Navier–Stokes equations', *Int. j. numer. methods fluids*, in press.
19. J. Farmer and L. Martinelli, 'A fast multigrid method for solving incompressible hydrodynamic problems with free surfaces', *AIAA Paper*, 1993.